Author/s:
Li, S;Ma, Y;Cui, J;Caruso, F;Ju, Y

Title:
Engineering poly(ethylene glycol) particles for targeted drug delivery

Date:
2024-01-23

Citation:
Li, S., Ma, Y., Cui, J., Caruso, F. & Ju, Y. (2024). Engineering poly(ethylene glycol) particles for targeted drug delivery. Chemical Communications, 60 (19), pp.2591-2604. https://doi.org/10.1039/d3cc06098e.

Persistent Link:
https://hdl.handle.net/11343/340197

ARTICLE

Engineering poly(ethylene glycol) particles for targeted drug delivery

Received 00th January 20xx,
Accepted 00th January 20xx

DOI: 10.1039/x0xx00000x

Shiyao Li,[a,b] Yutian Ma,[c] Jiwei Cui,[d] Frank Caruso[b] and Yi Ju*[a,b]

Poly(ethylene glycol) (PEG) is considered to be the "gold standard" among the stealth polymers employed for drug delivery. Using PEG to modify or engineer particles has thus gained increasing interest because of the ability to prolong blood circulation time and reduce nonspecific biodistribution *in vivo* of particles, owing to the low fouling and stealth properties of PEG. In addition, endowing PEG-based particles with targeting and drug-loading properties is essential to achieve enhanced drug accumulation at target sites *in vivo*. In this feature article, we focus on recent work on the synthesis of PEG particles, in which PEG is the main component in the particles. We highlight different synthesis methods used to generate PEG particles, the influence of the physiochemical properties of PEG particles on their stealth and targeting properties, and the application of PEG particles in targeted drug delivery.

1. Introduction

Poly(ethylene glycol) (PEG), a highly hydrophilic and electrically neutral polyether, is the most widely used polymer in the field of drug delivery.[1-4] It is also the key component in many nanomedicines that have been approved by the U.S. Food and Drug Administration for disease treatments and use in vaccines, such as Doxil,[5] Onpattro,[6] and SARS-CoV-2 mRNA vaccines.[7] It has been shown that PEG functionalization of nanoparticles (NPs), or PEGylation, can significantly improve the colloidal stability and pharmacokinetic properties of NPs by forming a hydration layer on the NPs and thereby reducing the adsorption of opsonins (i.e., extracellular proteins).[8,9] The molecular weight, density, and conformation of PEG chains can influence the stealth properties of the PEGylated NPs.[10-14] It is generally believed that PEG with a higher molecular weight or longer chains has a greater ability to inhibit the adsorption of opsonins than PEG with a lower molecular weight or shorter chains, resulting in NPs with better stealth properties.[8,11,15-17] However, there are contrasting reports on how the conformation of PEG chains affects the performance of NPs in biological environments. For example, Zhou *et al.* found that NPs with 20% PEG displaying a conformation close to the mushroom-to-brush transition demonstrated the longest blood circulation among the NPs studied comprising different PEG conformations.[18] This particular PEG conformation resulted in reduced NP uptake by non-Kupffer cells in the liver.[18] In contrast, Li *et al.* found that densely packed PEG chains with a brush conformation led to a lower nonspecific NP uptake by dendritic cells when compared with loosely packed PEG chains with a mushroom conformation.[16]

In addition to stealth properties, a challenge of nanoengineering particles is endowing them with targeting abilities. Targeting is important to deliver encapsulated cargoes to specific sites, thus potentially reducing side effects associated with off-target drug accumulation. Active targeting is commonly achieved by functionalizing NPs with targeting ligands. The functionalized NPs can then bind to specific receptors that are overexpressed at the target sites. A variety of targeting ligands with different sizes, specificities, and conjugation chemistries have been developed for different types of targeting NPs, including small molecules,[19-21] peptides,[22,23] aptamers,[24,25] and antibodies.[26,27] The targeting performance of NPs is influenced not only by the targeting ligands, but also by the stability and formation of a protein corona on the NPs in biological environments. Commonly used targeting ligands, such as antibodies and aptamers, have been shown to lose their targeting abilities after the formation of a protein corona on the NP surface.[28-30] There are also cases where protein coronas have been shown to improve targeting specificity and modulate immune cell association.[31,32] Therefore, it is essential to study how NPs interact with different components in biological environments (bio–nano interactions)[33] and to understand the influence of these bio–nano interactions on NP performance in biological models.

In the present feature article, we discuss our recent work on engineering micrometer- and nanometer-sized PEG particles, where (micrometer) particles are defined as having sizes of >1 μm. Unlike PEGylated particles, where the surface of the

[a] School of Science, RMIT University, Melbourne, Victoria 3000, Australia. E-mail: david.ju@rmit.edu.au
[b] Department of Chemical Engineering, The University of Melbourne, Parkville, Victoria 3010, Australia.
[c] Division of Pharmacoengineering and Molecular Pharmaceutics, Eshelman School of Pharmacy, University of North Carolina at Chapel Hill, Chapel Hill, NC 27599, USA.
[d] Key Laboratory of Colloid and Interface Chemistry of the Ministry of Education, School of Chemistry and Chemical Engineering, Shandong University, Jinan, Shandong 250100, China.

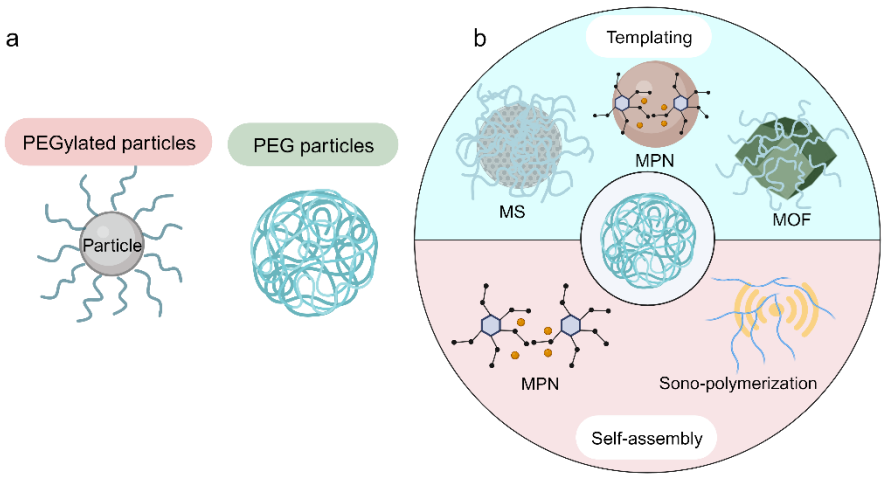

Fig. 1 Engineering of PEG particles. (a) Schematic of PEGylated and PEG particles. PEGylated particles are particles that are surface-modified with PEG, whereas PEG particles are mainly composed of PEG. (b) Various approaches have been developed for the development of PEG particles, which can be classified into templating methods—including MS templating, MPN templating, and MOF templating—and self-assembly methods—including MPN self-assembly and sono-polymerized self-assembly.

particles is functionalized with PEG, PEG particles are mainly composed of PEG (Fig. 1a). Over the past nine years, a number of engineering technologies have been devised to develop PEG particles with different sizes, structures, and building blocks. These technologies can be classified into templating methods, including mesoporous silica (MS) templating, metal–phenolic network (MPN) templating, and metal–organic framework (MOF) templating, and self-assembly methods, including MPN self-assembly and sono-polymerized self-assembly (Fig. 1b). Studies have investigated the bio–nano interactions and biomedical applications of PEG particles. Specifically, the influence of the physiochemical properties of PEG particles on their stealth properties has been investigated.[15,34-39] PEG particles have been endowed with targeting properties through their functionalization with various targeting ligands.[40-46] Some of these PEG particle systems have demonstrated successful targeted drug delivery *in vitro* and *in vivo*.[35,36,43-49] Advances on the engineering and bio-relevant applications of PEG particles over the last decade are displayed in Fig. 2. The strategies highlighted enable the engineering of PEG particles with tunable physiochemical properties, as well as stealth and targeting properties for investigating fundamental bio–nano interactions and for diverse biomedical applications, offering new opportunities for the development of stealth NP-based targeted drug delivery.

2. Engineering PEG particles

PEG particles can be engineered *via* different methods to endow them with various physiochemical properties. For example, using the MS templating, the size, shape, and structure of the engineered PEG particles can be tuned. Furthermore, the obtained PEG particles are highly hydrated and display excellent stealth properties.[15,38,50-52] In Sections 2.1–2.2, we highlight recent advances on engineering PEG particles through templating (Section 2.1) and self-assembly (Section 2.2) methods. More specifically, we discuss three types of templating methods, including MS templating, MPN templating, and MOF templating, as well as two self-assembly methods, including MPN self-assembly and sono-polymerized self-assembly.

2.1 Templating

2.1.1 MS templating

MS particles are widely used in catalysis,[53] enzyme immobilization,[54] template-based material synthesis,[55] and drug delivery[56-60] because of their high cargo loading efficiency, which is enabled by their well-ordered mesopores.[59,60] Furthermore, the size, morphology, and pore size of the MS particles can be tuned, which offers further opportunities for their use in engineering metal-, carbon-, or polymer-based replica particles.[61-66] MS template-based PEG particles (or capsules) can be prepared through surface-initiated polymerization or postinfiltration.[51] Compared with PEG particles prepared *via* surface-initiated polymerization, those engineered by postinfiltration exhibit superior stealth properties. As a result, PEG particles prepared from the latter method have gained increasing research interest in recent years.[15,65]

ARTICLE

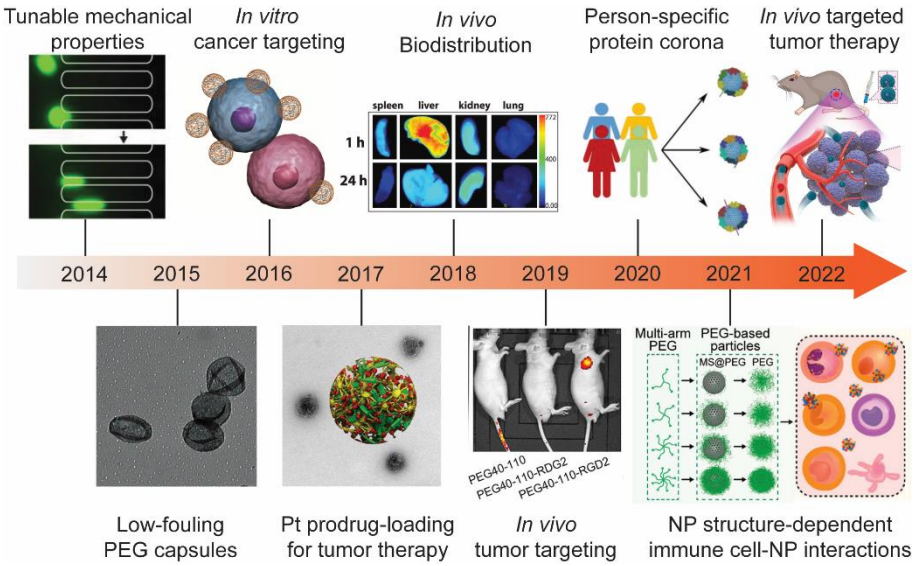

Fig. 2 Timeline providing key progress on the engineering and bio-relevant applications of PEG particles. Parts of this figure are adapted with permission from refs. [34,37,38,40,41,46,52,67,68]. Copyright 2014, 2017, and 2018 John Wiley and Sons, 2015, 2016, 2019, 2020, 2021, and 2022 American Chemical Society. PEG40-110, 110 nm PEG NPs prepared with 8-arm-PEG-NHS (40 kDa); PEG40-110-RDG2, 110 nm NPs prepared with an Arg-Asp-Gly-Phe-Lys (RDG)-to-8-arm-PEG-NHS (40 kDa) ratio of 2:1; PEG40-110-RGD2, 110 nm NPs prepared with an Arg-Gly-Asp-Phe-Lys (RGD)-to-8-arm-PEG-NHS (40 kDa) ratio of 2:1; MS@PEG, PEG-infiltrated MS particles; PEG (in 2021), PEG particles.

The assembly of PEG particles using MS templates and postinfiltration is accomplished by first infiltrating amine-functionalized PEG (PEG-NH_2) into MS particles through electrostatic interactions (MS@PEG particles). PEG-NH_2 is then cross-linked using PEG polymers functionalized with succinimidyl carboxyl methyl ester (PEG-NHS), followed by the dissolution of the MS template to yield PEG particles (Fig. 3a).[51] The obtained PEG particles showed a uniform size distribution, as assessed by transmission electron microscopy (TEM). Furthermore, the size of the PEG particles could be tuned from 100 nm to 1 μm by using MS template particles of different sizes (Fig. 3b–e).[15,41,42,52] The mechanical properties of the PEG particles were tuned by changing the concentration of the cross-linker and structure of the PEG polymers (Fig. 3f–i).[42] For instance, by changing the concentration of 8-arm-PEG-NHS from 0.5 to 4 mg mL^{-1}, the Young's modulus (E_Y) of the PEG particles changed from 0.2 to 3.3 kPa.[34] The increasing elasticities of the PEG particles were due to the increasing densities of PEG in the particles, as validated by an increase in the fluorescence intensity of the PEG particles (which contained 8-arm-PEG-NH_2 labeled with Alexa Fluor-488).[34] Increasing the arm number of PEG-NH_2 from 3 to 8 arms also resulted in a higher PEG loading amount, leading to an increase in the Young's modulus of the PEG particles from 1.5 to 14.9 kPa.[38]

2.1.2 MPN templating

MPNs are formed through the coordination between phenolic ligands and metal ions.[69] MPNs offer a facile strategy of surface coating and film engineering on various substrates, as well as engineering of self-assembled NPs owing to the universal adherent properties of the catechol and gallol groups of polyphenols.[67,70-75] Functionalization of PEG with phenolic groups enables PEG coating of different particles, including calcium carbonate ($CaCO_3$),[37,40] polymers,[39,76] and water-in-oil emulsions.[68,77] The size of PEG–MPN-coated particles can be tuned from micrometer to nanometer size (~50 nm) by using spherical templates of different sizes. For example, 3.2 μm PEG–MPN capsules were prepared by adding PEG–gallol and $FeCl_3{\cdot}6H_2O$ into an aqueous suspension containing 3.2 μm $CaCO_3$ particles, followed by the addition of tris-(hydroxymethyl)aminomethane buffer (pH 8.5) to raise the pH and subsequent removal of the $CaCO_3$ templates using ethylenediaminetetraacetic acid.[37] The PEG–MPN capsules showed pH-responsive disassembly at pH 5.0 while remaining stable at pH 7.4, due to the stoichiometric transitions of the PEG-polyphenol–Fe^{3+} complexes. Nanosized PEG–MPN capsules have been prepared using polymer NPs as templates. For example, gold NP-incorporated PEG–MPN (Au@PEG–MPN) nanocapsules with sizes ranging from 50 to 150 nm were prepared by using gold NP-incorporated benzene-1,4-dithiol (Au@BDT) NPs as templates (Fig. 4a–e).[39] These templates were synthesized *via* the supramolecular assembly of a polyphenol and self-polymerizable aromatic dithiol on gold NPs. The size of Au@BDT NPs could be tuned from 50 to 650 nm, and the phenolic groups incorporated in the Au@BDT NPs allowed for

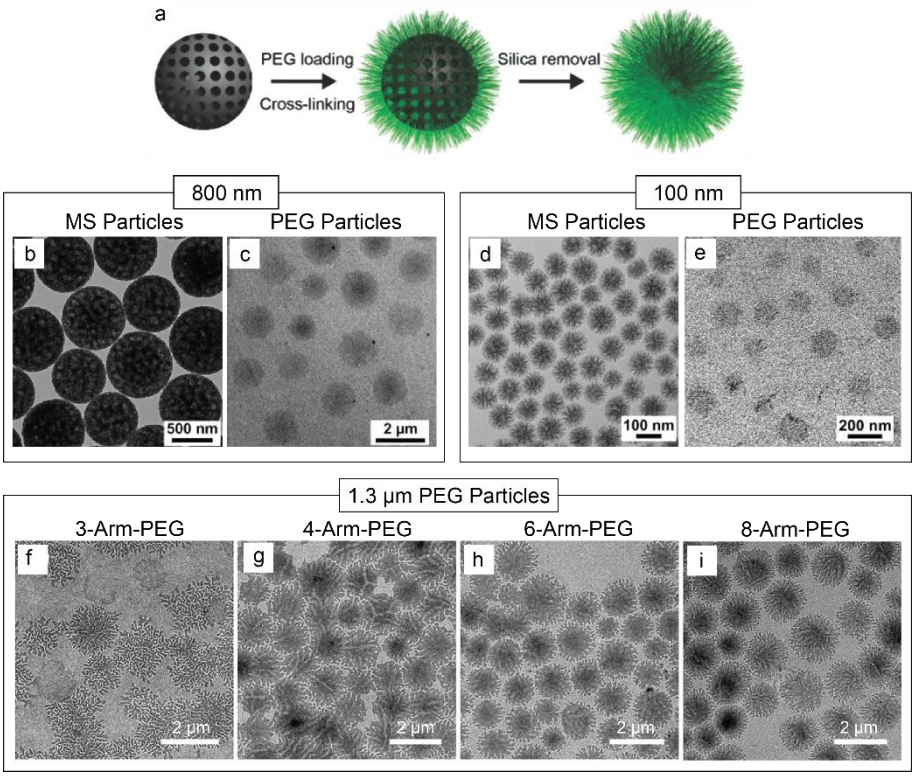

Fig. 3 Engineering and characterization of MS-based PEG particles. (a) Scheme of the synthesis of PEG particles *via* MS templating. Adapted with permission from ref. [34]. Copyright 2014 John Wiley and Sons. (b–e) TEM images of MS NPs of 800 nm (b) and 100 nm (d) in diameter, and PEG NPs of 800 nm (c) and 100 nm (e) in diameter prepared from the corresponding MS templates. (b–e) Adapted with permission from ref. [52]. Copyright 2020 American Chemical Society. (f–i) TEM images of PEG particles engineered from different PEG structures: 3-arm-PEG (f), 4-arm-PEG (g), 6-arm-PEG (h), and 8-arm-PEG (i). (f–i) Adapted with permission from ref. [38]. Copyright 2021 American Chemical Society.

the deposition of diverse materials onto the NP surface, thus serving as a spherical template for MPN coating. After removing the BDT templates using dimethylformamide, monodisperse Au@PEG–MPN nanocapsules of 50, 100, and 150 nm in size were obtained (Fig. 4c and e). MPN templating can also be used for engineering PEG–MPN-coated emulsions and PEG–MPN NPs. For example, PEG–MPN oil-in-water emulsions were engineered by first generating nanoemulsions of 100–250 nm in size *via* the ultrasonication of oleic acid in water.[68] Then PEG–polyphenol and Fe^{3+} were added to the nanoemulsions to form PEG–MPN films onto the surface of the nanoemulsions.[68] A series of PEG–MPN NPs composed of PEG–polyphenol and Mn^{2+} were engineered by adding an aqueous $MnCl_2$ and PEG–polyphenol solution (with different ratios) into a Triton X-100/1-hexanol mixture, raising the pH of the mixture to 8.0 for MPN cross-linking, and finally removing the templates by washing the NPs with 50% (v/v) ethanol/cyclohexane mixture and dispersing the NPs in Milli-Q water (Fig. 4f,g).[77] The NPs included solid and hollow NPs with sizes ranging from 30 to 50 nm. The size and morphology of the PEG–MPN NPs were controlled by varying the ratio of Mn^{2+} and gallol. At a low Mn^{2+}-to-gallol ratio (0.25:1), small (~30 nm) solid PEG–MPN NPs were obtained, whereas a high Mn^{2+}-to-gallol ratio (4:1) resulted in large hollow PEG–MPN nanocapsules of around 50 nm.

2.1.3 MOF templating

MOFs are obtained through the strong bonds (reticular synthesis) between metal ions and organic linkers.[78] MOFs exhibit uniform crystalline structures with high porosity and adjustable compositions and have been applied in many fields such as gas storage,[79] catalysis,[80] chemical sensing,[78,81] and drug delivery.[82,83] Among the different types of MOFs examined to date, zeolitic imidazolate frameworks (ZIFs), prepared through the coordination between metal ions and imidazole-based ligands, are the most extensively studied. ZIFs have been applied in drug delivery owing to their low toxicity, pH sensitivity, and endosomal escape properties,[83] and thus were chosen as the templates for PEG particle engineering.

PEG has been used as a mineralizing agent for the crystallization of ZIF-8 (PEG@ZIF-8) *via* interactions between the repeat units of the ethoxyl groups in PEG and metal ions.[36] PEG@ZIF-8 NPs

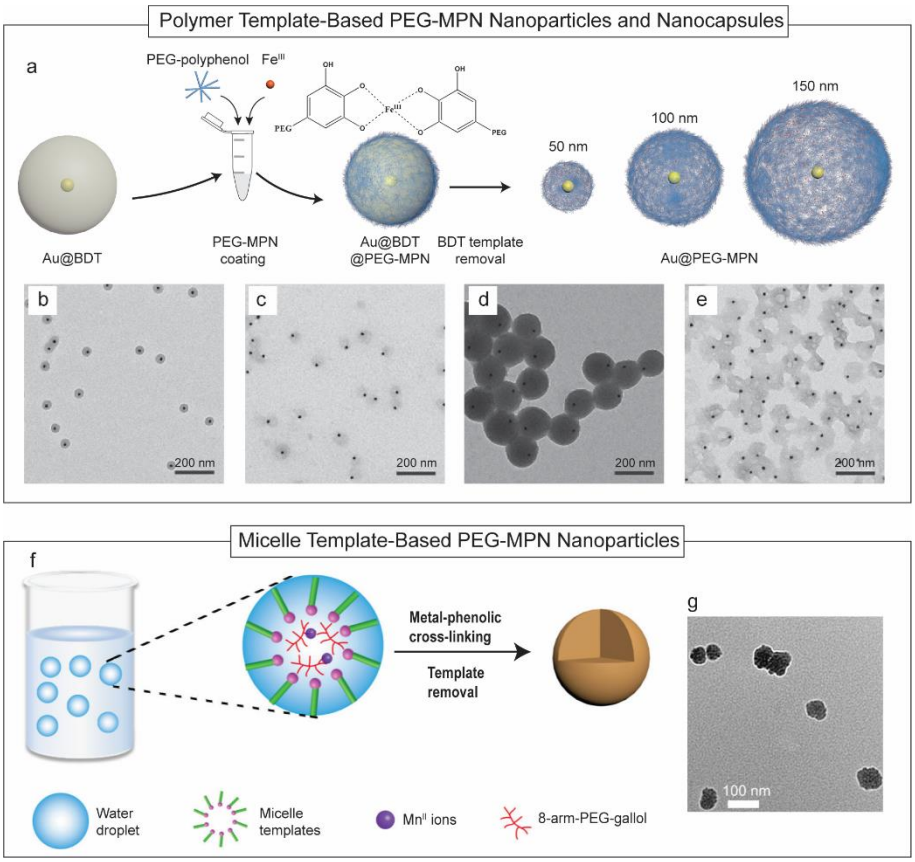

Fig. 4 MPN assembly of PEG-based NPs and nanocapsules. (a) Scheme of the preparation of PEG–MPN NPs and nanocapsules using Au@BDT as a polymer NP template. (b–e) TEM images of 50 nm (b) and 150 nm (d) Au@BDT@PEG–MPN NPs and corresponding 50 nm (c) and 150 nm (e) Au@PEG–MPN nanocapsules after template removal. (a–e) Adapted with permission from ref. [39]. Copyright 2021 American Chemical Society. (f) Scheme of the preparation of PEG–MPN NPs using micelles as a template. (g) TEM image of micelle template-based PEG–MPN NPs after template removal. (f,g) Adapted with permission from ref. [77]. Copyright 2021 American Chemical Society.

were synthesized by mixing 2-methylimidazole solution containing 8-arm-PEG-OH with zinc nitrate solution and stirring for 10 min.[36] The introduction of PEG molecules accelerated the prenucleation of ZIF-8 by forming clusters with Zn^{2+} and improved colloidal dispersity and stability in cell medium. Furthermore, the size of the PEG@ZIF-8 NPs could be varied from 60 to 590 nm by adjusting the concentration of PEG and incubation temperature. As reported in the literature, increasing the concentration of PEG or incubation temperature leads to smaller PEG@ZIF-8 NPs.[36] PEG NPs were obtained after ZIF template removal and PEG cross-linking by dispersing PEG@ZIF-8 in acetate buffer (50 mM, pH 5.5) containing 8-arm-PEG-2-nitro-5-thiobenzoate.[46] More recently, MOF templating has been broadened to employing 8-arm-PEG with different terminal groups, including 8-arm-PEG-thiol (8-arm-PEG-SH), 8-arm-PEG-maleimide (8-arm-PEG-MAL), 8-arm-PEG-4-nitrophenyl-2-(2-pyridyldithio)ethyl carbonate (8-arm-PEG-NDEC), and 8-arm-PEG-NH_2 (Fig. 5a–d).[49] Different building blocks were loaded into ZIF-8 NPs to form 8-arm-PEG-SH@ZIF-8 NPs, 8-arm-PEG-MAL@ZIF-8 NPs, 8-arm-PEG-NDEC@ZIF-8 NPs, and 8-arm-PEG-NH_2@ZIF-8 NPs (Fig. 5e–h). PEG NPs were obtained by dispersing the PEG@ZIF-8 NPs in acetate buffer containing different cross-linkers on the basis of different cross-linking strategies (Fig. 5i–l). Furthermore, automated mineralization of PEG@ZIF-8 NPs was achieved by mixing the PEG solution and 2-methylimidazole solution containing cargoes from two separate channels of a microfluidic chip, and the reaction was initiated upon mixing the obtained mixture with $Zn(NO_3)_2$ on another microfluid chip.[48] The automated synthesis of PEG@ZIF-8 NPs is expected to facilitate large-scale processes for future personalized synthesis of therapeutics.

2.2 Self-assembly

2.2.1 MPN self-assembly

In addition to surface coating, MPNs also offer a platform for designing self-assembled nanocomplexes of diverse compositions owing to the wide selection of available building

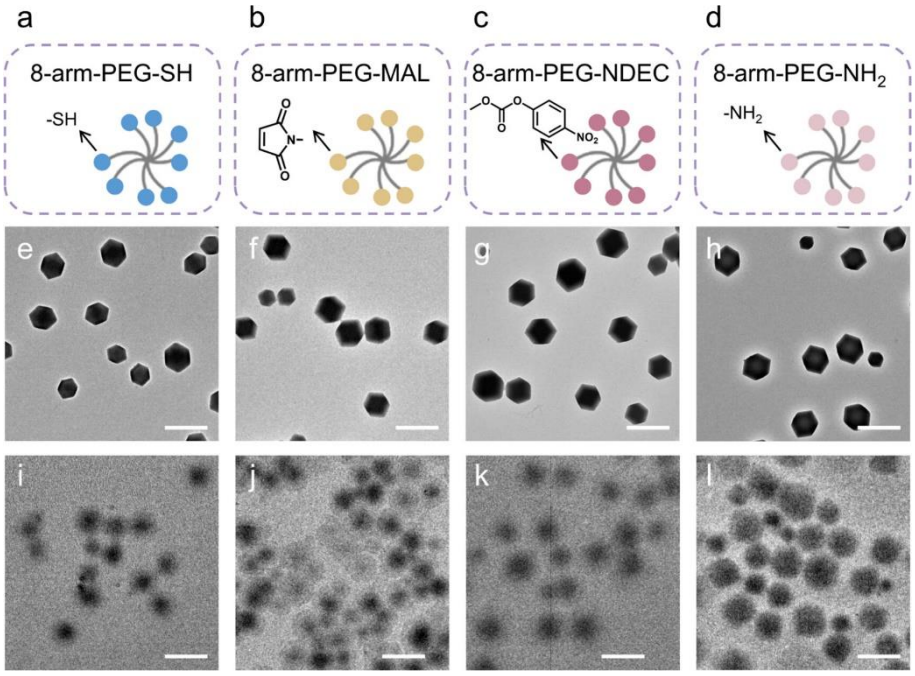

Fig. 5 Preparation of MOF-based PEG NPs using different cross-linking strategies. Illustrations of (a) 8-arm PEG-SH, (b) 8-arm-PEG-MAL, (c) 8-arm-PEG-NDEC, and (d) 8-arm-PEG-NH_2. TEM images of (e) 8-arm-PEG-SH@ZIF-8 NPs, (f) 8-arm-PEG-MAL@ZIF-8 NPs, (g) 8-arm-PEG-NDEC@ZIF-8 NPs, and (h) 8-arm-PEG-NH_2@ZIF-8 NPs. TEM images of the corresponding PEG NPs (after template removal) obtained using different cross-linking strategies: (i) thioldisulfide exchange, (j) click chemistry, (k) amidation reaction, and (l) Schiff base reaction. Scale bars: 1 μm. (a–l) Reproduced with permission from ref.[49]. Copyright 2023 American Chemical Society.

blocks (*i.e.*, polyphenols and metal ions), as well as the strong interactions of polyphenols with diverse molecules, including aromatic molecules,[84] peptides,[85] proteins,[75,86,87] and nucleic acids.[75,88,89] For example, 100 nm PEG–MPN nanocomplexes containing platinum (Pt) prodrugs were assembled through the coordination of PEG–polyphenol and Pt prodrug–polyphenol with Fe^{3+}. Specifically, $FeCl_3$, PEG–polyphenol, and Pt prodrug–polyphenol were first mixed in hexane, Triton X-100, and hexanol to form water-in-oil emulsions. Subsequently, the pH was adjusted to 8.5 to form MPN tris-complexes and the nanocomplexes were stabilized by washing with ethanol and water.[67]

2.2.2 Sono-polymerized self-assembly

Sono-polymerization is a sonication-initiated polymerization technique that has attracted significant research interest as this process can be conducted under catalyst- and organic solvent-free conditions.[90-93] The underlying mechanism of this process involves the ultrasound-assisted production of free radicals through acoustic cavitation. These radicals can attack the carbon double bonds of water-soluble monomers and initiate polymerization.[92-96] The synthesis of sono-polymerized self-assembled PEG NPs was demonstrated through the polymerization of acrylate-terminal methoxy PEG-2k (ACLT-PEG_{2k}) monomers under ultrasonication conditions.[35] The process was optimized by adjusting the sonication frequency, power, and temperature (*i.e.*, 412 kHz, 40 W, and 40–50 °C) to generate the highest level of hydroxyl radicals.[35] The polymerization rate was dependent on the monomer concentration and the PEG molecular weight. Increasing the concentration of ACLT-PEG_{2k} from 10 to 20% generated PEG macromonomer with increasing molecular weight from 32.6 to 1377 kDa. Increasing the molecular weight of the PEG monomer from 2000 to 5000 Da reduced the polymerization time from 20 to 7 min.[35] Recently, sono-polymerized PEG NPs were prepared by initiating the polymerization of ACLT-PEG monomers within water-in-oil microemulsions and subsequently removing the oil phase.[45] Microemulsions were generated using Tween 80 and Span 80, and their size was tuned by changing the ratios of the oil, surfactants, and water, thereby enabling control over the size of the PEG NPs from 20 to 500 nm (Fig. 6a–c).[45] The obtained PEG NPs showed a uniform size distribution, as assessed by atomic force microscopy (AFM) (Fig. 6d and e).

3. Bio–nano interaction studies and biomedical applications of PEG particles

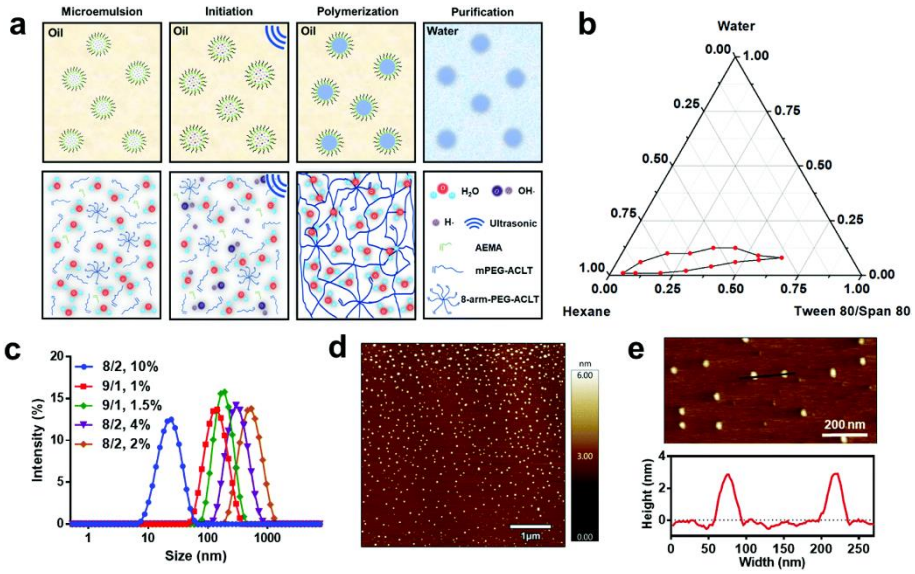

Fig. 6 Synthesis of PEG NPs using sono-polymerization. (a) Scheme of the sono-microemulsion polymerization process. The water-in-oil microemulsions are first generated, followed by the initiation of the ultrasonication process and polymerization of PEG monomers. Finally, PEG NPs are obtained by removing the microemulsions. (b) Pseudo-ternary phase diagram of a microemulsion system composed of a hexane oil phase, a surfactant (Span 80 and Tween 80) phase, and a water phase containing PEG and AEMA. (c) Size distribution of microemulsions, which is dependent on the weight ratio of oil and surfactants (8/2 or 9/1) and the weight percentage of the water phase (1–10%). (d) AFM image of PEG NPs with an average diameter of 25 nm. (e) Magnified AFM image of PEG NPs and corresponding height profile along the black line in the AFM image. (a–e) Reproduced with permission from ref. [45]. Copyright 2022 The Royal Society of Chemistry.

The application of different methods enables the engineering of particles with various properties and advantages suitable for diverse applications and studies. For instance, MS templating allows precise control of the physiochemical properties of PEG particles, such as size, shape, and structure, making MS-based PEG particles good models for investigating bio–nano interactions.[15,65,97,98] Furthermore, MPN self-assembly offers the flexibility to load various therapeutic cargoes into PEG particles during the assembly process owing to the adherent properties of phenolic groups with different molecules.[67,99-102] Sections 3.1–3.3 summarize recent studies on bio–nano interactions and the biomedical applications of PEG particles, including their low-fouling, stealth, and targeting properties, as well as their drug-loading capabilities.

3.1 Low-fouling and stealth properties

PEG is the most commonly used polymer for stealth coating and it has been shown to increase the colloidal stability of particles and reduce nonspecific protein adsorption and cell–particle associations. For example, the amount of protein adsorbed on a PEG–MPN film after incubating the film with human blood serum for 1 h at 37 °C was lower (*i.e.*, ~1.8 ng mm^{-2}) than that observed on a tannic acid (TA)-based MPN film under the same conditions (i.e., ~8.6 ng mm^{-2}), indicating that PEG coating could reduce nonspecific protein adsorption.[37] Cell association studies were conducted on 3.2 μm PEG–MPN capsules and TA-based MPN capsules to compare their stealth properties. After incubating the MPN capsules with HeLa cells at 37 °C for 24 h at a cell-to-capsule ratio of 1:50, the PEG–MPN capsules showed lower cell association (<2%) than the TA-based MPN capsules (>60%).[37] A similar trend was observed with smaller capsules—100 nm PEG–MPN nanocapsules showed lower cell association (~20%) than TA-based MPN nanocapsules of the same size (~60%) after incubation for 24 h with RAW 264.7 cells at a cell-to-capsule ratio of 1:1000.[39]

The stealth properties of PEG particles are influenced by several factors such as the molecular weight and structure of PEG, as well as the size and structure of the PEG particles. To understand the influence of particle structure and molecular weight of PEG on the stealth properties, whole blood assays

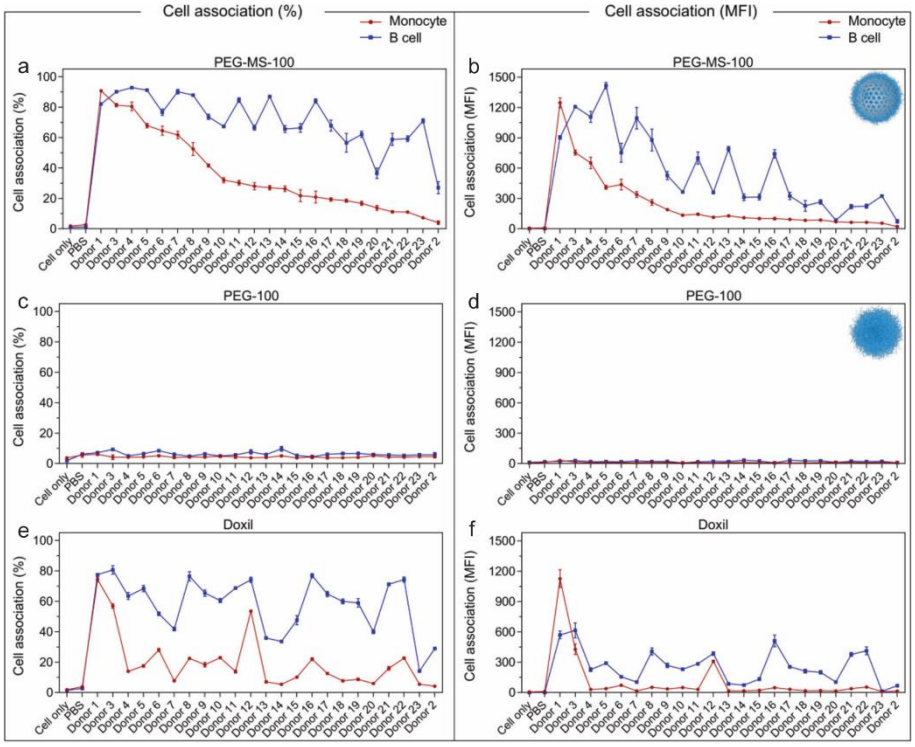

Fig. 7 Association of monocytes and B cells with different types of NPs, as assessed in terms of percentage (a,c,e) and median fluorescence intensity (MFI) (b,d,f): 100 nm MS@PEG NPs (PEG-MS-100) (a,b); 100 nm PEG NPs (PEG-100) (c,d); and Doxil NPs (e,f). (a–f) Adapted with permission from ref. [52]. Copyright 2020 American Chemical Society.

were conducted on 1000 nm MS@PEG and PEG particles prepared using 10, 20, and 40 kDa 8-arm-PEG-NH_2. In this study, micrometer-sized MS templates were selected for ease of sample preparation and characterization, including particle morphology, structure, elasticity and protein corona compositions.[38] The results demonstrated that 40kDa-PEG NPs exhibited reduced association (<20%) with monocytes and granulocytes, which are the major cells responsible for pathogen elimination in blood, when compared with the 10kDa-PEG NPs. This observation was likely due to the longer PEG chains in 40kDa-PEG NPs that could form thicker hydration layers on their surface, thus providing higher resistance to the adsorption of proteins and association with the cell membrane.[103]

Compared with PEG particles, MS@PEG particles showed significantly higher association with monocytes and granulocytes (>50%).[15] Similar results were observed for PEG–MPN nanocapsule system, where 100 and 150 nm Au@BDT@PEG–MPN core–shell NPs displayed higher association (>70%) with monocytes compared with the Au@PEG–MPN nanocapsules (<40%). The higher cell association displayed by the template-incorporated PEG particles was attributed to the differences in particle elasticity, as the templates (MS particles for PEG@MS particles and Au@BDT NPs for Au@BDT@PEG–MPN core–shell NPs) had higher rigidity.[15,39] This was further confirmed by a systematic study performed on PEG particles with different elasticities, ranging from 1.5 to 14.9 kPa, and prepared using 3-, 4-, 6-, and 8-arm PEG-NH_2.[38] Blood assays were also conducted to study the influence of the mechanical properties of PEG particles on their interactions with blood immune cells. Among the PEG particles prepared, 8-arm PEG particles displayed the highest association with granulocytes, monocytes, and B cells in both whole blood and washed blood (plasma-removed blood) conditions, indicating that the formation of a protein corona is not the main factor that influences cell association. Instead, cell association may rely on the direct interactions between cell membranes and PEG chains, which are influenced by the mechanical properties of the PEG chains.[38]

The effect of particle size on bio–nano interactions was studied using PEG–MPN nanocapsules of 50, 100, and 150 nm in size and performing *ex vivo* whole blood assays and *in vivo* experiments in rat models. The largest PEG–MPN nanocapsules (*i.e.*, 150 nm) showed the highest cell association with neutrophils and monocytes, and had the shortest elimination half-life.[39] The results were consistent with a previous study

that showed that 500 nm PEG NPs had a shorter elimination half-life than 280 nm PEG NPs.[15]

Importantly, the stealth properties of PEG-based NPs have been found to be person-specific and can be modulated by biomolecular coronas. A systematic study of NP–immune cell interactions was performed wherein 100 nm MS@PEG NPs, 100 nm PEG NPs, and clinically relevant PEGylated doxorubicin-encapsulated liposomes (Doxil) were incubated with plasma from 23 healthy donors before incubating with washed peripheral blood mononuclear cells. The PEG NPs consistently showed negligible cell association with monocytes and B cells, irrespective of the plasma donor. In contrast, MS@PEG NPs and Doxil showed significant variance in their association with monocytes and B cells across the 23 donors (Fig. 7). Proteomics analysis of the biomolecular coronas identified the presence of key immunoglobulin and complement proteins that strongly correlated with the cell association patterns observed.[52]

The consistently low immune cell interactions of PEG NPs have been attributed to their enhanced stealth properties, compared to PEGylated NPs. Although studies have shown that PEGylation has improved the stealth properties of NPs, many studies have indicated that the presence of PEG leads to the generation of anti-PEG antibodies and the subsequent accelerated blood clearance (ABC) of PEGylated NPs after repeated administration.[104,105] Our recent study has shown that the increase in anti-PEG antibodies observed after mRNA-1273 vaccination correlates with the enhanced uptake of the PEGylated NPs by blood phagocytes.[106,107] However, in contrast, the PEG NPs engineered through MOF templating did not show significant ABC phenomenon,[46] possibly due to their low adsorption of opsonins, including anti-PEG antibodies, in blood.

3.2 Targeting

PEG particles can be endowed with targeting properties through, for example, the surface functionalization of polysaccharides, peptides, or antibodies. Hyaluronic acid (HA)-functionalized PEG–MPN capsules were engineered to target CD44-overexpressed cancer cells by incorporating HA-polyphenol into the building blocks.[40] HA has a strong binding affinity for CD44 receptor. The resulting HA/PEG–MPN capsules showed targeting capabilities for MDA-MB-231 (CD44+) cells and displayed a similar level of nonspecific association with BT474 (CD44−) cells to that displayed by PEG-MPN capsules without HA functionalization.[40] HA was also integrated into PEG NPs prepared using MOF templating by adding HA-SH into the building blocks during NP synthesis.[46] The resulting HA–PEG NPs showed specific targeting to 4T1 (CD44+) cells and exhibited low association with RAW 264.7 (CD44−) cells.[46] Targeting PEG particles were also engineered through the functionalization of anti-PEG bispecific antibodies (BsAbs), which have dual specificity for PEG and cancer targets.[108] A previous study demonstrated the functionalization of PEG particles with anti-PEG-anti-epidermal growth factor receptor (EGFR) BsAbs (PEG-EGFR particles) to target EGFR-overexpressed cancer cells. The functionalization of the BsAbs was characterized by the merged fluorescence of the Alex Fluor-488-labeled BsAbs and Alex Fluor-633-labeled PEG particles (Fig. 8a–c). Cell targeting experiments showed that 110 nm PEG-EGFR NPs exhibited high targeting (>90%) of MDA-MB-468 (EGFR+) cells, while displaying <5% association with CHO-K1 (EGFR−) cells (Fig. 8d,e).

Similarly, PEG NPs prepared by sono-polymerization were also functionalized with anti-PEG-anti-human epidermal growth factor receptor-2 (HER2) BsAbs and displayed a high targeting ability toward breast cancer cells (SKBR3) that overexpress HER2 receptors.[45] However, PEG-EGFR NPs did not show significantly higher tumor accumulation *in vivo* compared with PEG NPs without BsAb functionalization.[42] The difference in the targeting ability of PEG-EGFR NPs between *in vitro* and *in vivo* experiments could result from the complexity of the *in vivo* environment, which is challenging to replicate *in vitro*.

Functionalization of PEG particles with cyclic peptides has also been used to endow particles with targeting properties. For example, PEG NPs were functionalized with targeting cyclic peptides (Arg-Gly-Asp-Phe-Lys, abbreviated as RGD) or control cyclic peptides (Arg-Asp-Gly-Phe-Lys, abbreviated as RDG) to generate PEG-RGD or PEG-RDG NPs by preincubating 8-arm-PEG-NHS with RGD or RDG during NP synthesis. The RGD sequence can be recognized by $\alpha_v\beta_3$ integrins that are overexpressed at angiogenic tumor sites and thus can be used as a targeting ligand. The control cyclic peptides are composed of the same amino acids as RGD but the sequence of the amino acids differs and is not recognized by the $\alpha_v\beta_3$ integrins. The 110 nm PEG-RGD NPs prepared with an RGD-to-8-arm-PEG-NHS (40 kDa) ratio of 2:1 (denoted as PEG40-110-RGD2) displayed strong targeting to the $\alpha_v\beta_3$-overexpressed U87 MG cells *in vitro* and showed higher tumor accumulation *in vivo* compared with PEG NPs (Fig. 8f,g).[41] Similarly, PEG capsules prepared *via* emulsion templating and PEG NPs prepared by sono-polymerization were successfully functionalized with RGD cyclic peptides and showed high targeting to U87 MG cells *in vitro*.[35,44]

3.3 Drug delivery

An anticancer Pt prodrug, c,c,t-[$Pt(NH_3)_2Cl_2(OH)$-($O_2CCH_2CH_2CO_2H$)], was loaded into PEG NPs prepared through microemulsion sono-polymerized self-assembly. The drug and 30% 2-aminoethyl methacrylate hydrochloride (AEMA) were

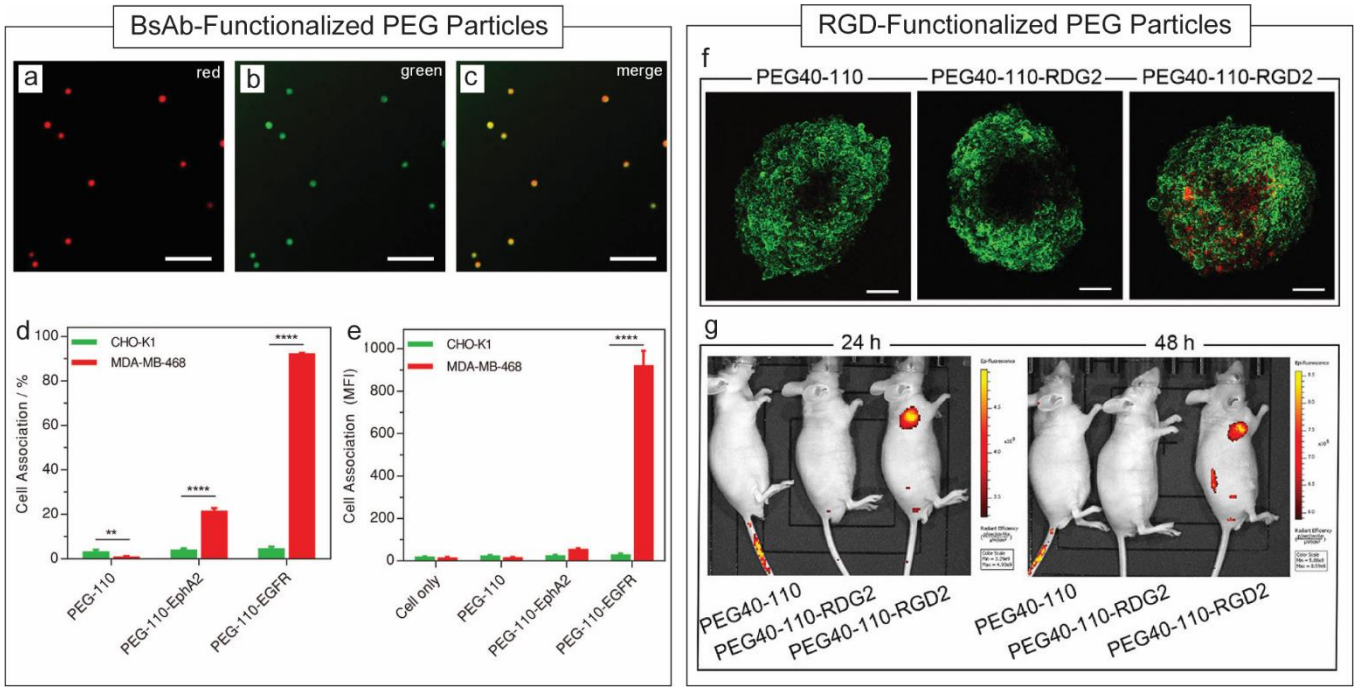

Fig. 8 Targeting studies of PEG NPs functionalized with different targeting ligands. (a–c) Confocal laser scanning microscopy images of (a) 1000 nm PEG NPs labeled with Alex Fluor-633 (red), (b) 1000 nm PEG NPs functionalized with Alex Fluor-488-labeled anti-PEG/anti-EGFR BsAbs, and (c) merged channels of red and green fluorescence. Scale bars: 10 µm. (d,e) Association of MDA-MB-468 and CHO-K1 cells with 110 nm PEG NPs (PEG-110) functionalized with ephrin type-A receptor 2 (EphA2) (PEG-110-EphA2) or EGFR BsAbs (PEG-110-EGFR). Cell association with particles was determined by flow cytometry and represented as (d) percentage or (e) MFI. (a–e) Adapted with permission from ref. [42]. Copyright 2019 John Wiley and Sons. (f,g) Targeting of 110 nm PEG NPs assembled with 40 kDa 8-arm-PEG-NH_2 (PEG40-110) and functionalized with RDG2 (PEG40-110-RDG2) or RGD2 (PEG40-110-RGD2) in a multicellular spheroid model (f) and *in vivo* (g). (f) Cell membranes (green) were stained with wheat germ agglutinin–Alex Fluor-488 conjugate and NPs (red) were labeled with Alex Fluor-647. Scale bars: 100 µm. (g) Time-dependent *in vivo* fluorescence images of Alex Fluor-647-labeled PEG40-110, PEG40-110-RDG2, and PEG40-110-RGD2 NPs intravenously injected in mice with U-87 MG xenograft tumors. (f,g) Adapted with permission from ref. [41]. Copyright 2019 American Chemical Society.

introduced into the building blocks during the sono-polymerization process, where the role of AEMA is to conjugate the drug into the NPs.[35] The Pt prodrug was also loaded into the self-assembled PEG–MPN NPs, and the PEG–MPN NPs showed passive tumor accumulation and inhibition of tumor growth *in vivo*.[67]

Chlorin e6 was loaded into PEG-RGD NPs engineered through MS templating for targeted photodynamic therapy. The obtained chlorin e6-loaded PEG-RGD NPs showed high targeting and high cytotoxicity toward U-87 MG cells under 660 nm laser irradiation.[43] Similarly, indocyanine green (ICG) was encapsulated into the PEG NPs prepared *via* microemulsion-based sono-polymerized self-assembly by introducing ICG-NHS and AEMA into the sonication process. The ICG@PEG NPs were functionalized with BsAbs for specific targeting.[45] The obtained ICG@PEG-BsAb NPs induced over 50% cell apoptosis in the targeted cells under laser irradiation, whereas in the absence of laser irradiation, the PEG NPs and ICG-BsAbs showed negligible cell death, which was at a similar level to that displayed by the blank cells.

Doxorubicin (DOX), an anti-cancer drug that can induce cell apoptosis through inhibiting RNA and DNA production, has also been encapsulated into PEG particles. For example, PEG-RGD capsules prepared *via* emulsion templating were dispersed in NaOH solution (pH 8) and mixed with DOX in the dark for 24 h at room temperature for DOX loading.[44] The obtained DOX-loaded PEG-RGD capsules showed a similar level of cell cytotoxicity toward the targeted cells to that displayed by free DOX.[44] DOX was also loaded into PEG NPs prepared by MOF templating by adding DOX during the mineralization process.[36] At pH 7.4, the obtained DOX-loaded PEG@ZIF-8 NPs showed <20% DOX release, whereas at pH 6.0, ~90% release was observed after 24 h incubation owing to the pH-dependent degradability of the NPs. Cell viability experiments showed that the DOX-loaded PEG@ZIF-8 NPs were more toxic to the cancer cells than the free DOX. Furthermore, the PEG@ZIF-8 NPs (without DOX) of the same NP concentration showed negligible effect on the cells. These results indicated the high drug delivery efficacy and high biocompatibility of the DOX-loaded PEG@ZIF-8 NPs.[36] More recently, DOX-loaded PEG-HA (DOX@PEG-HA)

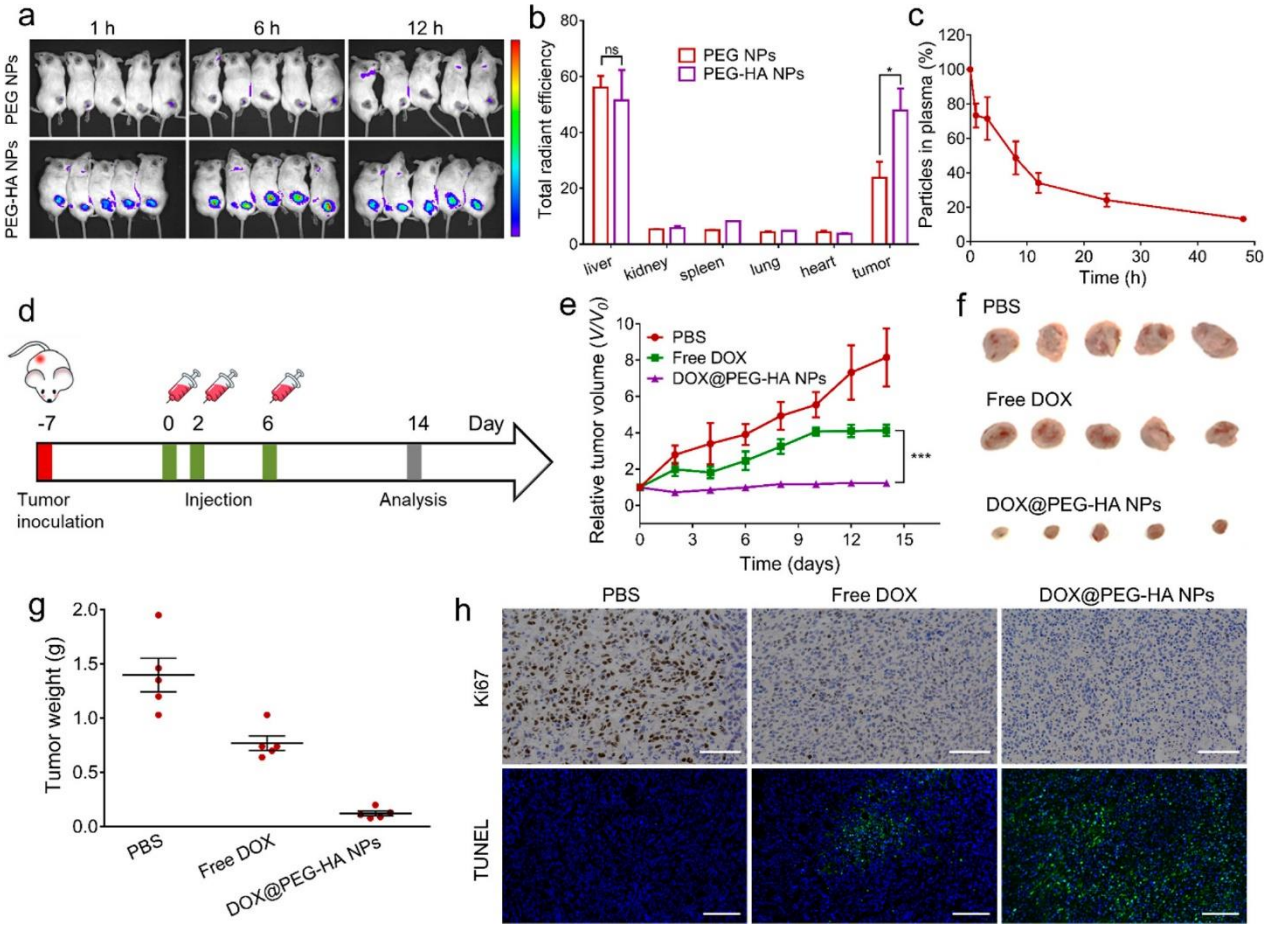

Fig. 9 *In vivo* tumor targeting studies of MOF-based PEG NPs. (a) *In vivo* fluorescence images of 4T1 tumor-bearing mice after injection of Cy5-labeled PEG NPs or PEG-HA NPs. (b) Biodistribution of PEG NPs and PEG-HA NPs at 12 h postintravenous administration. Data are presented as the mean ± standard deviation (n = 5); *P < 0.05; ns, not significant, as determined by student's t-test. (c) Circulation time of PEG-HA NPs in blood. (d) Schematic illustration of the experimental process used to assess tumor inhibition. (e) Changes in tumor volume of the different treatment groups (PBS, free DOX, and DOX@PEG-HA NPs). Data are presented as the mean ± standard deviation (n = 5); ***P < 0.001 as determined by one-way analysis of variance for the three groups. (f) Photographs and (g) mass of excised tumors from representative mice from different treatment groups. (h) Ki67 and TUNEL images of tumor sections after different treatments to identify cell proliferation and apoptosis, respectively. Scale bars: 100 µm. Reproduced with permission from ref. [46]. Copyright 2022 American Chemical Society.

NPs were reported to effectively inhibit tumor growth *in vivo*, as confirmed by the weights of the harvested tumors and Ki67 and TUNEL staining on the tumor sections (Fig. 9).[46] The relative tumor volume of the DOX@PEG-HA-treated mice (~1.2) was significantly lower than those of the phosphate-buffered saline (PBS)-treated mice (~8.1) and free-DOX-treated mice (~4.0). Ki67 and TUNEL staining demonstrated that the DOX@PEG-HA NPs inhibited tumor proliferation and that the number of apoptotic tumor cells in the DOX@PEG-HA group was lower than that in the free DOX group.

PEG@ZIF-8-based vaccine NPs were successfully engineered by coencapsulating an antigen (*i.e.*, ovalbumin (OVA)) and an adjuvant (*i.e.*, cytosine–phosphate–guanine oligodeoxynucleotides (CpG)) into NPs (OVA-CpG@ZIF-8 NPs).[47] The OVA-CpG@ZIF-8 NPs were synthesized by adding a mixture of OVA and CpG during mineralization. OVA in the vaccine NPs showed a pH-dependent release similar to the release of DOX from DOX-loaded PEG@ZIF-8 NPs—at pH 7.2 and pH 5.5, <25% and >80% release were observed, respectively, after incubation for 24 h. The immunostimulatory activity of the PEG@ZIF-8-based vaccine NPs-treated mice was assessed by enzyme-linked immunosorbent assay and flow cytometry to measure the level of immunoglobulin G (IgG) in the mouse serum, the secretion of cytokines in the mouse primary spleen lymphocytes, and the proportion of CD4+ and CD8+ T cells. The results showed that the OVA-CpG@ ZIF-8 NP group displayed significantly increased IgG titers, CD4+ and CD8+ T cell subpopulations, and secretion

levels of interleukin-2, interferon-γ, and tumor necrosis factor-α relative to the groups treated with free OVA or the mixture of free OVA and free CpG.[47]

4. Summary and outlook

In this feature article, we discussed our recent work in the synthesis of PEG particles with controlled physiochemical properties using templating and self-assembly approaches. Among the engineering technologies discussed in this feature article, MS templating enables precise control of the sizes and mechanical properties of the PEG particles with high stealth. However, some barriers currently impede their further applications for drug delivery, including the lack of stimuli responsiveness and challenges in drug loading during particle synthesis. MPN templating enables PEG coating on various templates, benefiting from the high-affinity properties of phenolic groups on different surfaces. Moreover, MPN assembly provides a facile and robust approach for engineering self-assembled drug-loaded PEG NPs and the PEG–MPN NPs have shown potential in cancer therapy,[67,99,100,109,110] immunotherapy,[101] and radiotherapy.[102] MOF templating has enabled the engineering of PEG NPs with controlled physiochemical properties, including size, and elasticity, and stimuli-responsiveness, and they have exhibited promising stealth properties, particularly the inhibition of ABC effects, and targeted drug delivery abilities. Sono-polymerized self-assembly offers an efficient approach to engineering PEG NPs of tunable size in a one-pot process. However, this approach may not be suitable for loading drugs that are sensitive to ultrasonication and heat.[92]

Future studies may focus on engineering PEG NPs with controlled drug-release properties for the treatment of specific diseases. Despite progress achieved in balancing the targeting and stealth properties of PEG NPs, it remains challenging to determine the optimal balance between retaining enhanced stealth properties of the NPs and endowing the NPs with high targeting properties. Therefore, a deeper understanding of how different approaches, such as developing stimuli-responsive and cleavable stealth NPs, can influence NP performance is needed for designing advanced NPs. New NP design strategies will provide further opportunities to understand the fundamentals of bio–nano interactions and will pave the way for accelerating the development of the next generation of NP-based drug delivery systems.

Conflicts of interest

There are no conflicts to declare.

Acknowledgements

This research was funded by the Australian Research Council (ARC) through the Discovery Project scheme (DP210103114). Y.J. acknowledges support received through the ARC Discovery Early Career Researcher Award scheme (DE230101542), a Victoria Fellowship from The Victoria State Government, and an RMIT Vice-Chancellor's Postdoctoral Fellowship from RMIT University. F.C. acknowledges the award of a National Health and Medical Research Council (NHMRC) Leadership Fellowship (GNT2016732). J.C. acknowledges support from the National Natural Science Foundation of China (22072075 and 22372091).

Notes and references

1. R. Greenwald, *J. Controlled Release*, 2001, **74**, 159.
2. P. Bailon and C.-Y. Won, *Expert Opin. Drug Delivery*, 2009, **6**, 1.
3. A. A. D'souza and R. Shegokar, *Expert Opin. Drug Delivery*, 2016, **13**, 1257.
4. A. Kolate, D. Baradia, S. Patil, I. Vhora, G. Kore and A. Misra, *J. Controlled Release*, 2014, **192**, 67.
5. Y. Barenholz, *J. Controlled Release*, 2012, **160**, 117.
6. A. Akinc, M. A. Maier, M. Manoharan, K. Fitzgerald, M. Jayaraman, S. Barros, S. Ansell, X. Du, M. J. Hope and T. D. Madden, *Nat. Nanotechnol.*, 2019, **14**, 1084.
7. L. Schoenmaker, D. Witzigmann, J. A. Kulkarni, R. Verbeke, G. Kersten, W. Jiskoot and D. J. Crommelin, *Int. J. Pharm.*, 2021, **601**, 120586.
8. T. U. Wani, S. N. Raza and N. A. Khan, *Polym. Bull.*, 2019, **77**, 3865.
9. Kenry, T. Yeo, P. N. Manghnani, E. Middha, Y. Pan, H. Chen, C. T. Lim and B. Liu, *ACS Nano*, 2020, **14**, 4509.
10. S. S. Pai, B. Hammouda, K. Hong, D. C. Pozzo, T. M. Przybycien and R. D. Tilton, *Bioinorg. Chem.*, 2011, **22**, 2317.
11. S. R. Benhabbour, H. Sheardown and A. Adronov, *Macromolecules*, 2008, **41**, 4817.
12. L. Xiao, J. Li, G. Peng and G. Huang, *React. Funct. Polym.*, 2020, **156**, 104736.
13. C. Cruje and D. Chithrani, *J. Nanomed. Res.*, 2014, **1**, 8.
14. T. Kanamaru, K. Sakurai and S. Fujii, *Biomacromolecules*, 2022, **23**, 3909.
15. J. Cui, R. De Rose, K. Alt, S. Alcantara, B. M. Paterson, K. Liang, M. Hu, J. J. Richardson, Y. Yan, C. M. Jeffery, R. I. Price, K. Peter, C. E. Hagemeyer, P. S. Donnelly, S. J. Kent and F. Caruso, *ACS Nano*, 2015, **9**, 1571.
16. M. Li, S. Jiang, J. Simon, D. Passlick, M. L. Frey, M. Wagner, V. Mailander, D. Crespy and K. Landfester, *Nano Lett.*, 2021, **21**, 1591.
17. P. Zhang, Z. Zhang, D. Wang, J. Hao and J. Cui, *ACS Macro Lett.*, 2020, **9**, 1478.
18. H. Zhou, Z. Fan, P. Y. Li, J. Deng, D. C. Arhontoulis, C. Y. Li, W. B. Bowne and H. Cheng, *ACS Nano*, 2018, **12**, 10130.
19. B. Bahrami, M. Mohammadnia-Afrouzi, P. Bakhshaei, Y. Yazdani, G. Ghalamfarsa, M. Yousefi, S. Sadreddini, F. Jadidi-Niaragh and M. Hojjat-Farsangi, *Tumor Biol.*, 2015, **36**, 5727.
20. M. J. Henley and A. N. Koehler, *Nat. Rev. Drug Discovery*, 2021, **20**, 669.
21. N. Kaur, P. Popli, N. Tiwary and R. Swami, *J. Controlled Release*, 2023, **355**, 417.
22. Z. Jiang, J. Guan, J. Qian and C. Zhan, *Biomater. Sci.*, 2019, **7**, 461.

23. C. D. Spicer, C. Jumeaux, B. Gupta and M. M. Stevens, *Chem. Soc. Rev.*, 2018, **47**, 3574.
24. J. Guo, X. Gao, L. Su, H. Xia, G. Gu, Z. Pang, X. Jiang, L. Yao, J. Chen and H. Chen, *Biomaterials*, 2011, **32**, 8010.
25. Z. Fu and J. Xiang, *Int. J. Mol. Sci.*, 2020, **21**, 9123.
26. Q. Dai, Y. Yan, C.-S. Ang, K. Kempe, M. M. Kamphuis, S. J. Dodds and F. Caruso, *ACS Nano*, 2015, **9**, 2876.
27. Y. Cui, P. Cui, B. Chen, S. Li and H. Guan, *Drug Dev. Ind. Pharm.*, 2017, **43**, 519.
28. K. Zarschler, K. Prapainop, E. Mahon, L. Rocks, M. Bramini, P. M. Kelly, H. Stephan and K. A. Dawson, *Nanoscale*, 2014, **6**, 6046.
29. B. S. Varnamkhasti, H. Hosseinzadeh, M. Azhdarzadeh, S. Y. Vafaei, M. Esfandyari-Manesh, Z. H. Mirzaie, M. Amini, S. N. Ostad, F. Atyabi and R. Dinarvand, *Int. J. Pharm.*, 2015, **494**, 430.
30. M. Tonigold, J. Simon, D. Estupinan, M. Kokkinopoulou, J. Reinholz, U. Kintzel, A. Kaltbeitzel, P. Renz, M. P. Domogalla, K. Steinbrink, I. Lieberwirth, D. Crespy, K. Landfester and V. Mailander, *Nat. Nanotechnol.*, 2018, **13**, 862.
31. Y. Ju, Q. Dai, J. Cui, Y. Dai, T. Suma, J. J. Richardson and F. Caruso, *ACS Appl. Mater. Interfaces*, 2016, **8**, 22914.
32. S. Li, Y. Ju, J. Zhou, M. Faria, C. S. Ang, A. J. Mitchell, Q. Z. Zhong, T. Zheng, S. J. Kent and F. Caruso, *J. Mater. Chem. B*, 2022, **10**, 7607.
33. Y. Ju, C. J. Kim and F. Caruso, *Acc. Chem. Res.*, 2023, **56**, 1826.
34. J. Cui, M. Bjornmalm, K. Liang, C. Xu, J. P. Best, X. Zhang and F. Caruso, *Adv. Mater.*, 2014, **26**, 7295.
35. Z. Gao, H. Zhu, X. Li, P. Zhang, M. Ashokkumar, F. Cavalieri, J. Hao and J. Cui, *ACS Macro Lett.*, 2019, **8**, 1285.
36. Q. Yu, Y. Tian, M. Li, Y. Jiang, H. Sun, G. Zhang, Z. Gao, W. Zhang, J. Hao, M. Hu and J. Cui, *Chem. Commun.*, 2020, **56**, 11078.
37. Y. Ju, J. Cui, M. Müllner, T. Suma, M. Hu and F. Caruso, *Biomacromolecules*, 2015, **16**, 807.
38. J. Song, Y. Ju, T. H. Amarasena, Z. Lin, S. Mettu, J. Zhou, M. A. Rahim, C. S. Ang, C. Cortez-Jugo, S. J. Kent and F. Caruso, *ACS Nano*, 2021, **15**, 10025.
39. S. Li, Y. Ju, J. Zhou, K. F. Noi, A. J. Mitchell, T. Zheng, S. J. Kent, C. J. H. Porter and F. Caruso, *ACS Appl. Mater. Interfaces*, 2021, **13**, 35494.
40. Y. Ju, J. Cui, H. Sun, M. Mullner, Y. Dai, J. Guo, N. Bertleff-Zieschang, T. Suma, J. J. Richardson and F. Caruso, *Biomacromolecules*, 2016, **17**, 2268.
41. J. Cui, K. Alt, Y. Ju, S. T. Gunawan, J. A. Braunger, T. Y. Wang, Y. Dai, Q. Dai, J. J. Richardson, J. Guo, M. Bjornmalm, C. E. Hagemeyer and F. Caruso, *Biomacromolecules*, 2019, **20**, 3592.
42. J. Cui, Y. Ju, Z. H. Houston, J. J. Glass, N. L. Fletcher, S. Alcantara, Q. Dai, C. B. Howard, S. M. Mahler and A. K. Wheatley, *Advanced healthcare materials*, 2019, **8**, 1801607.
43. X. Fu, H. Sun, G. Zhang, K. Zhao, Y. Tian, Z. Gao, J. Cui and Q. Yu, *Colloids Surf., A*, 2020, **606**, 125394.
44. S. Yang, F. Ding, Z. Gao, J. Guo, J. Cui and P. Zhang, *Polymers (Basel)*, 2020, **12**, 1124.
45. Z. Gao, X. Li, K. Zhao, H. Geng, P. Zhang, Y. Ju, P. Huda, C. B. Howard, K. J. Thurecht, M. Ashokkumar, J. Hao and J. Cui, *Chem. Commun.*, 2022, **58**, 7777.
46. Y. Tian, Z. Gao, N. Wang, M. Hu, Y. Ju, Q. Li, F. Caruso, J. Hao and J. Cui, *J. Am. Chem. Soc.*, 2022, **144**, 18419.
47. G. Zhang, X. Fu, H. Sun, P. Zhang, S. Zhai, J. Hao, J. Cui and M. Hu, *ACS Appl. Mater. Interfaces*, 2021, **13**, 13978.
48. M. Wu, L. Xia, Y. Li, D. Yin, J. Yu, W. Li, N. Wang, X. Li, J. Cui, W. Chu, Y. Cheng and M. Hu, *Chin. Chem. Lett.*, 2022, **33**, 497.
49. Y. Tian, Z. Gao, M. Li, M. Hu, J. Hao and J. Cui, *Chem. Mater.*, 2023, **35**, 5593.
50. J. Cui, J. J. Richardson, M. Bjornmalm, M. Faria and F. Caruso, *Acc. Chem. Res.*, 2016, **49**, 1139.
51. J. Cui, M. Bjornmalm, Y. Ju and F. Caruso, *Langmuir*, 2018, **34**, 10817.
52. Y. Ju, H. G. Kelly, L. F. Dagley, A. Reynaldi, T. E. Schlub, S. K. Spall, C. A. Bell, J. Cui, A. J. Mitchell, Z. Lin, A. K. Wheatley, K. J. Thurecht, M. P. Davenport, A. I. Webb, F. Caruso and S. J. Kent, *ACS Nano*, 2020, **14**, 15723.
53. M. Hartmann, *Chem. Mater.*, 2005, **17**, 4577.
54. R. A. Sheldon, *Adv. Synth. Catal.*, 2007, **349**, 1289.
55. J. Lee, J. Kim and T. Hyeon, *Adv. Mater.*, 2006, **18**, 2073.
56. Slowing, II, J. L. Vivero-Escoto, C. W. Wu and V. S. Lin, *Adv. Drug Delivery Rev.*, 2008, **60**, 1278.
57. J. Cui, Y. Yan, Y. Wang and F. Caruso, *Adv. Funct. Mater.*, 2012, **22**, 4718.
58. M. Vallet-Regí, *ISRN Mater. Sci.*, 2012, **2012**, 1.
59. Z. Xu, X. Ma, Y.-E. Gao, M. Hou, P. Xue, C. M. Li and Y. Kang, *Mater. Chem. Front.*, 2017, **1**, 1257.
60. M. Manzano and M. Vallet‐Regí, *Adv. Funct. Mater.*, 2020, **30**, 1902634.
61. I. I. Slowing, J. L. Vivero-Escoto, B. G. Trewyn and V. S. Y. Lin, *J. Mater. Chem.*, 2010, **20**, 7924.
62. S. H. Wu, C. Y. Mou and H. P. Lin, *Chem. Soc. Rev.*, 2013, **42**, 3862.
63. L. Huang, S. J. Wind and S. P. O'Brien, *Nano Lett.*, 2003, **3**, 299.
64. T. A. Crowley, K. J. Ziegler, D. M. Lyons, D. Erts, H. Olin, M. A. Morris and J. D. Holmes, *Chem. Mater.*, 2003, **15**, 3518.
65. D. Song, J. Cui, H. Sun, T. H. Nguyen, S. Alcantara, R. De Rose, S. J. Kent, C. J. H. Porter and F. Caruso, *ACS Appl. Mater. Interfaces*, 2017, **9**, 33683.
66. Y. Ju, H. Liao, J. J. Richardson, J. Guo and F. Caruso, *Chem. Soc. Rev.*, 2022, **51**, 4287.
67. Y. Dai, J. Guo, T. Y. Wang, Y. Ju, A. J. Mitchell, T. Bonnard, J. Cui, J. J. Richardson, C. E. Hagemeyer, K. Alt and F. Caruso, *Adv. Healthcare Mater.*, 2017, **6**, 1700467.
68. Q. A. Besford, Y. Ju, T. Y. Wang, G. Yun, P. Cherepanov, C. E. Hagemeyer, F. Cavalieri and F. Caruso, *Small*, 2018, **14**, 1802342.
69. H. Ejima, J. J. Richardson, K. Liang, J. P. Best, M. P. van Koeverden, G. K. Such, J. Cui and F. Caruso, *Science*, 2013, **341**, 154.
70. H. Ejima, J. J. Richardson and F. Caruso, *Polym. J.*, 2014, **46**, 452.
71. J. Guo, Y. Ping, H. Ejima, K. Alt, M. Meissner, J. J. Richardson, Y. Yan, K. Peter, D. von Elverfeldt, C. E. Hagemeyer and F. Caruso, *Angew Chem. Int. Ed.*, 2014, **53**, 5546.
72. M. A. Rahim, K. Kempe, M. Müllner, H. Ejima, Y. Ju, M. P. van Koeverden, T. Suma, J. A. Braunger, M. G. Leeming, B. F. Abrahams and F. Caruso, *Chem. Mater.*, 2015, **27**, 5825.

73. J. Guo, B. L. Tardy, A. J. Christofferson, Y. Dai, J. J. Richardson, W. Zhu, M. Hu, Y. Ju, J. Cui, R. R. Dagastine, I. Yarovsky and F. Caruso, *Nat. Nanotechnol.*, 2016, **11**, 1105.
74. H. Ejima, J. J. Richardson and F. Caruso, *Nano Today*, 2017, **12**, 136.
75. J. Chen, S. Pan, J. Zhou, Z. Lin, Y. Qu, A. Glab, Y. Han, J. J. Richardson and F. Caruso, *Adv. Mater.*, 2022, **34**, e2108624.
76. C.-J. Kim, F. Ercole, E. Goudeli, S. K. Bhangu, J. Chen, M. Faria, J. F. Quinn and F. Caruso, *Chem. Mater.*, 2022, **34**, 7468.
77. G. Lin, C. Cortez-Jugo, Y. Ju, Q. A. Besford, T. M. Ryan, S. Pan, J. J. Richardson and F. Caruso, *Biomacromolecules*, 2021, **22**, 612.
78. H. Furukawa, K. E. Cordova, M. O'Keeffe and O. M. Yaghi, *Science*, 2013, **341**, 1230444.
79. D. Alezi, Y. Belmabkhout, M. Suyetin, P. M. Bhatt, Ł. J. Weseliński, V. Solovyeva, K. Adil, I. Spanopoulos, P. N. Trikalitis and A.-H. Emwas, *J. Am. Chem. Soc.*, 2015, **137**, 13308.
80. Q. Wang and D. Astruc, *Chem. Rev.*, 2019, **120**, 1438.
81. R. Freund, O. Zaremba, G. Arnauts, R. Ameloot, G. Skorupskii, M. Dinca, A. Bavykina, J. Gascon, A. Ejsmont, J. Goscianska, M. Kalmutzki, U. Lachelt, E. Ploetz, C. S. Diercks and S. Wuttke, *Angew Chem. Int. Ed.*, 2021, **60**, 23975.
82. J. Zhuang, A. P. Young and C. K. Tsung, *Small*, 2017, **13**, 1700880.
83. Q. Wang, Y. Sun, S. Li, P. Zhang and Q. Yao, *RSC Adv.*, 2020, **10**, 37600.
84. J. Zhou, Z. Lin, M. Penna, S. Pan, Y. Ju, S. Li, Y. Han, J. Chen, G. Lin, J. J. Richardson, I. Yarovsky and F. Caruso, *Nat. Commun.*, 2020, **11**, 4804.
85. Y. Han, R. P. M. Lafleur, J. Zhou, W. Xu, Z. Lin, J. J. Richardson and F. Caruso, *J. Am. Chem. Soc.*, 2022, **144**, 12510.
86. Y. Han, Z. Lin, J. Zhou, G. Yun, R. Guo, J. J. Richardson and F. Caruso, *Angew Chem. Int. Ed.*, 2020, **59**, 15618.
87. Y. Han, J. Zhou, Y. Hu, Z. Lin, Y. Ma, J. J. Richardson and F. Caruso, *ACS Nano*, 2020, **14**, 12972.
88. Y. Qu, Y. Ju, C. Cortez‐Jugo, Z. Lin, S. Li, J. Zhou, Y. Ma, A. Glab, S. J. Kent and F. Cavalieri, *Small*, 2020, **16**, 2002750.
89. Y. Qu, R. De Rose, C. J. Kim, J. Zhou, Z. Lin, Y. Ju, S. K. Bhangu, C. Cortez-Jugo, F. Cavalieri and F. Caruso, *Angew Chem. Int. Ed.*, 2023, **62**, e202214935.
90. T. G. McKenzie, F. Karimi, M. Ashokkumar and G. G. Qiao, *Chem. Eur. J.*, 2019, **25**, 5372.
91. I. Zaborniak and P. Chmielarz, *Macromol. Chem. Phys.*, 2019, **220**, 1900285.
92. A. R. S. Kumar, A. Padmakumar, U. Kalita, S. Samanta, A. Baral, N. K. Singha, M. Ashokkumar and G. Qiao, *Prog. Mater. Sci.*, 2023, 101113.
93. S. K. Bhangu, S. Fernandes, G. L. Beretta, S. Tinelli, M. Cassani, A. Radziwon, M. Wojnilowicz, S. Sarpaki, I. Pilatis, N. Zaffaroni, G. Forte, F. Caruso, M. Ashokkumar and F. Cavalieri, *Adv. Mater.*, 2022, **34**, 2107964.
94. D.-H. Roh, H. Shin, H.-T. Kim and T.-H. Kwon, *ACS Appl. Mater. Interfaces*, 2021, **13**, 61598.
95. B. M. Teo, S. W. Prescott, G. J. Price, F. Grieser and M. Ashokkumar, *J. Phys. Chem. B*, 2010, **114**, 3178.
96. T. G. McKenzie, E. Colombo, Q. Fu, M. Ashokkumar and G. G. Qiao, *Angew Chem. Int. Ed.*, 2017, **56**, 12302.
97. J. A. Braunger, M. Bjornmalm, N. A. Isles, J. Cui, T. M. Henderson, A. J. O'Connor and F. Caruso, *Biomater. Sci.*, 2017, **5**, 267.
98. D. Song, J. Cui, Y. Ju, M. Faria, H. Sun, C. B. Howard, K. J. Thurecht and F. Caruso, *ACS Appl. Mater. Interfaces*, 2019, **11**, 28720.
99. Z. Zhang, B. Li, L. Xie, W. Sang, H. Tian, J. Li, G. Wang and Y. Dai, *ACS Nano*, 2021, **15**, 16934.
100. Z. Zhang, W. Sang, L. Xie, W. Li, B. Li, J. Li, H. Tian, Z. Yuan, Q. Zhao and Y. Dai, *Angew Chem. Int. Ed.*, 2021, **60**, 1967.
101. L. Xie, J. Li, G. Wang, W. Sang, M. Xu, W. Li, J. Yan, B. Li, Z. Zhang, Q. Zhao, Z. Yuan, Q. Fan and Y. Dai, *J. Am. Chem. Soc.*, 2022, **144**, 787.
102. J. Yan, G. Wang, L. Xie, H. Tian, J. Li, B. Li, W. Sang, W. Li, Z. Zhang and Y. Dai, *Adv. Mater.*, 2022, **34**, e2105783.
103. L. Shi, J. Zhang, M. Zhao, S. Tang, X. Cheng, W. Zhang, W. Li, X. Liu, H. Peng and Q. Wang, *Nanoscale*, 2021, **13**, 10748.
104. E. T. Dams, P. Laverman, W. J. Oyen, G. Storm, G. L. Scherphof, J. W. Van der Meer, F. H. Corstens and O. C. Boerman, *J. Pharmacol. Exp. Ther.*, 2000, **292**, 1071.
105. T. Ishida, R. Maeda, M. Ichihara, K. Irimura and H. Kiwada, *J. Controlled Release*, 2003, **88**, 35.
106. Y. Ju, W. S. Lee, E. H. Pilkington, H. G. Kelly, S. Li, K. J. Selva, K. M. Wragg, K. Subbarao, T. H. O. Nguyen, L. C. Rowntree, L. F. Allen, K. Bond, D. A. Williamson, N. P. Truong, M. Plebanski, K. Kedzierska, S. Mahanty, A. W. Chung, F. Caruso, A. K. Wheatley, J. A. Juno and S. J. Kent, *ACS Nano*, 2022, **16**, 11769.
107. Y. Ju, J. M. Carreno, V. Simon, K. Dawson, F. Krammer and S. J. Kent, *Nat. Rev. Immunol.*, 2023, **23**, 135.
108. C. B. Howard, N. Fletcher, Z. H. Houston, A. V. Fuchs, N. R. Boase, J. D. Simpson, L. J. Raftery, T. Ruder, M. L. Jones, C. J. de Bakker, S. M. Mahler and K. J. Thurecht, *Adv. Healthcare Mater.*, 2016, **5**, 2055.
109. J. Wang, W. Sang, Z. Yang, Z. Shen, Z. Wang, O. Jacobson, Y. Chen, Y. Wang, M. Shao, G. Niu, Y. Dai and X. Chen, *J. Mater. Chem. B*, 2019, **7**, 5688.
110. W. Sang, Z. Zhang, G. Wang, L. Xie, J. Li, W. Li, H. Tian and Y. Dai, *Adv. Funct. Mater.*, 2022, **32**.

Table of Content Graph